OPTICS

Cross-wavelength invisibility integrated with various invisibility tactics

Su Xu[1]*†, Fu-Yan Dong[1]*, Wen-Rui Guo[2], Dong-Dong Han[1], Chao Qian[3,4], Fei Gao[3,4], Wen-Ming Su[2], Hongsheng Chen[3,4]†, Hong-Bo Sun[1,5]†

As a superior self-protection strategy, invisibility has been a topic of long-standing interest in both academia and industry, because of its potential for intriguing applications that have only appeared thus far in science fiction. However, due to the strong dispersion of passive materials, achieving cross-wavelength invisibility remains an open challenge. Inspired by the natural ecological relationship between transparent midwater oceanic animals and the cross-wavelength detection strategy of their predators, we propose a cross-wavelength invisibility concept that integrates various invisibility tactics, where a Boolean metamaterial design procedure is presented to balance divergent material requirements over cross-scale wavelengths. As proof of concept, we experimentally demonstrate longwave cloaking and shortwave transparency simultaneously through a nanoimprinting technique. Our work extends the concept of stealth techniques from individual invisibility tactics targeting a single-wavelength spectrum to an integrated invisibility tactic targeting a cross-wavelength applications and may pave the way for development of cross-wavelength integrated metadevices.

INTRODUCTION

In the open ocean, becoming transparent, thus allowing light to pass through the body, provides a superior self-protection strategy for midwater prey (*1*), such as the hyperiid amphipod crustacean *Cystisoma* in Fig. 1A. As *Cystisoma* is almost transparent except for some necessary organs, such as the eyes, its substantially reduced scattering cross section enables it to avoid detection by most predators. However, a few predators can still use cross-spectra vision (*2*) to detect and successfully attack this kind of prey because of the special capabilities of the predator eyes. If a prey could break the balanced prey-predator interaction by concealing itself completely from the cross-spectra vision of predators, then the possibility of survival in the midwater ocean would be much higher.

Inspired by this ecological relationship, we propose a cross-wavelength invisibility concept that integrates longwave cloaking and shortwave transparency simultaneously, which is almost impossible through any individual invisibility tactic with passive materials (*3*–*11*). This ecological relationship–inspired cross-wavelength invisibility philosophy complements the existing two mainstream methodologies, i.e., chameleon-like adaptive camouflage (*3*–*6*) and wave-bypassing invisibility cloaking (*7*–*11*). It is even beyond nature, as we break the aforementioned ecological relationship artificially by hiding the transparent "prey" from the cross-spectra vision of "predators." Therefore, this invisibility philosophy is of significance to practical stealth technologies. For example, a transparent stealth aircraft or vehicle that has appeared only in science fiction thus far could be emulated in the laboratory. In such an aircraft or vehicle, the pilot or driver inside can see the surrounding dynamics freely without worrying about being detected by outside microwave radar systems. To realize this cross-wavelength invisibility concept in practice, the divergent material parameters required for various invisibility tactics should be well balanced in an individual metastructure, a problem that has received little attention in previous research (*3*–*6*, *12*–*27*).

Here, we adopt a Boolean metamaterial design procedure to combine the functionalities of each micro/nanostructure required for different invisibility tactics. As proof of concept, we successfully demonstrate an optically transparent microwave cloak that integrates longwave cloaking and shortwave transparency simultaneously. The device is constructed of macroscopic metallic networks (extremely high local electrical conductivity) with microscopic silver/nickel (Ag/Ni) wires (extremely low global optical conductivity) through nanoimprinting fabrication (*28*). The experimental results demonstrate a substantial reduction in the scattering cross section in the microwave regime from 6 to 10 GHz and optical transparency from 400 to 760 nm.

RESULTS

A schematic of the optically transparent microwave cloak is illustrated in Fig. 1B. With a transparent body, the cloak should be penetrated by visible light (blue and yellow rays) with negligible loss, decreasing the optical scattering cross section and allowing the internal observer to simultaneously see outside freely. Meanwhile, both the amplitude and phase of the reflected microwave beam should be the same as those for the ground reflection case when microwave waves (green rays) interact with the metasurface cloak. For comparison with the schematic view, the sample realized in practice is shown in Fig. 1C. The geometrical dimensions of the fabricated cloak are $D = 114.8$ mm, $d = 42$ mm, and $h = 21$ mm. The cloak is fully transparent, and the internal object (i.e., the metallic badge with the words "Jilin University") can be seen from the outside. This phenomenon indicates that the internal observer can see outside freely and that the visible dimensions of the cloak are obviously decreased compared to a fully opaque cloak. Our optically transparent microwave invisibility cloak consists of two metasurfaces imprinted on flexible polyethylene terephthalate

[1]State Key Laboratory of Integrated Optoelectronics, College of Electronic Science and Engineering, Jilin University, Changchun 130012, China. [2]Printable Electronics Research Centre, Suzhou Institute of Nano-Tech and Nano-Bionics, Chinese Academy of Sciences, Suzhou 215123, China. [3]Interdisciplinary Center for Quantum Information, State Key Laboratory of Modern Optical Instrumentation, Zhejiang University, Hangzhou 310027, China. [4]ZJU-Hangzhou Global Scientific and Technological Innovation Center, The Electromagnetics Academy, College of Information Science & Electronic Engineering, Zhejiang University, Hangzhou 310027, China. [5]State Key Laboratory of Precision Measurement Technology and Instruments, Department of Precision Instrument, Tsinghua University, Haidian, Beijing 100084, China.
*These authors contributed equally to this work.
†Corresponding author. Email: xusu@jlu.edu.cn (S.X.); hansomchen@zju.edu.cn (H.C.); hbsun@tsinghua.edu.cn (H.-B.S)

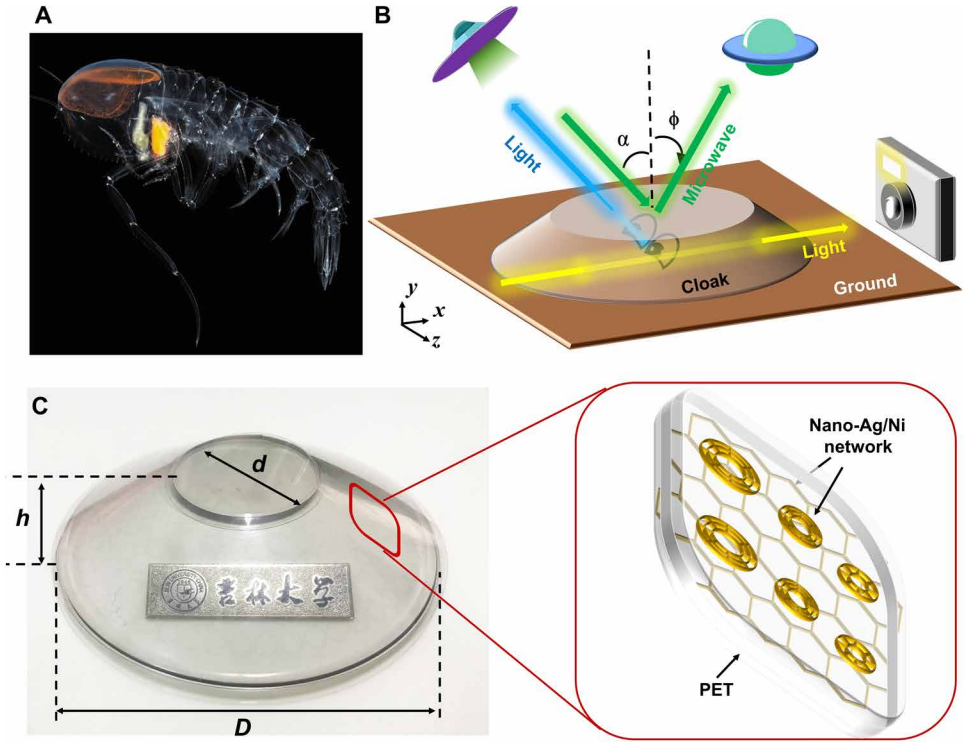

Fig. 1. Biological inspiration, schematic view, and practical sample of an optically transparent microwave invisibility cloak. (**A**) Photo of the hyperiid amphipod crustacean *Cystisoma*, which lives in a midwater oceanic environment. Photo credit: David Liittschwager, reproduced from (*1*), used with permission. (**B**) Schematic of the optically transparent microwave invisibility cloak. This cloak can conceal objects with preserved phases and microwave amplitudes (green beams with incident angle α and reflected angle ϕ). At the same time, the cloak can ensure that internal observers see external aircraft clearly (blue beams) and can decrease the optical scattering (yellow beams). (**C**) Example of the optically transparent microwave invisibility cloak. The metallic badge with the words "Jilin University" represents an object concealed inside. The enlarged section presents a schematic view of the metasurfaces composed of nano-Ag/Ni networks. Photo credit: Fu-Yan Dong, Jilin University.

(PET) films and isolated by a curved transparent PET spacer with a relative permittivity of 3.37 at 1 MHz (*29*). The thickness of the PET films is 0.15 mm, while the thickness of the spacer is 2.16 mm for the top cover and 1.8 mm for the sidewall of the cloak. The inner-layer metasurface acts as a perfect electric conductor (PEC) boundary, while the ring resonators on the outer-layer metasurface provide proper phase compensation and amplitude preservation effects.

We start the design by engineering the electromagnetic response for microwave invisibility. According to the generalized Snell's law (*10*, *18*), metallic ring resonators should provide a phase response $\Delta\Phi = \pi - 2k_0h_u \cos\alpha$ to compensate for the phase error induced by the height of the bump. Here, k_0 and h_u represent the wave number in free space and the height of the unit cell center, respectively. In total, eight kinds of ring resonators with periodicity p = 6 mm are used to build the cloak and are named ring N (N = 1, 2, …, 8) from the bottom to the top (see fig. S1). The angle θ at which a microwave encounters a ring resonator on the sidewall can be written as $\theta = \left|\alpha \pm \tan^{-1}\frac{h}{(D-d)}\right|$ (*18*), and the incident direction–dependent phase response is studied in Fig. 2 (A and B), for the cases of transverse electric (TE)– and transverse magnetic (TM)–polarized incidence, respectively. One can see that the phase responses are close to the ideal phase shift at θ = 10°, 20°, 30°, and 40° for the TE case, while the phase responses of the resonators have a slight deviation with different θ for the TM case. Since our carpet cloak design is based on phase compensation of the metasurface (*10*, *18*), which reconstructs the reflected wave so that it is the same as the wave reflected from the original ground plane, it does not have the apparent height problem and the lateral shift of scattering waves (*30*).

Designing only unit cells for microwave invisibility is not enough to realize cross-wavelength invisibility. On the one hand, microwave cloaking structures producing the proper phase shift and preserved amplitude response require a material with ultrahigh electrical conductivity, which is usually found in natural homogeneous metals. On the other hand, the metastructures should present an extremely high transmitted light intensity, which requires ultralow optical conductivity. To match the material requirements of an optically transparent microwave cloak, we prepare a transparent silver mesh to achieve extremely high global electrical conductivity and ultralow global optical conductivity as the first step. A schematic view of this silver mesh with a square lattice in air is shown in Fig. 2C. The silver structure is described by the Drude model (*31*). That is, the relative permittivity can be expressed by $\epsilon(\omega) = 1 - \frac{\omega_p^2}{\omega(\omega + i\omega_c)}$, where the plasma frequency $\omega_p = 1.39 \times 10^{16}$ s^{-1} and the collision frequency $\omega_c = 3.23 \times 10^{13}$ s^{-1}. The bulk conductivity of silver can be expressed by $\sigma = \frac{\sigma_0}{1 + \omega^2/\omega_c^2}$, where $\sigma_0 = \epsilon_0\omega_p^2/\omega_c$ is the DC conductivity of silver. For the case with fixed lattice periodicity p_m = 200 μm and thickness t_m = 8 μm, the effective conductivity at microwave frequencies and the sheet resistance of the metallic mesh can be estimated by $\sigma_{microw} = \sigma\frac{w_m}{p_m}$ and $R_{s,mesh} = \frac{p_m}{\sigma t_m w_m}$, respectively (*32*). For the case where w_m is greater than the wavelength

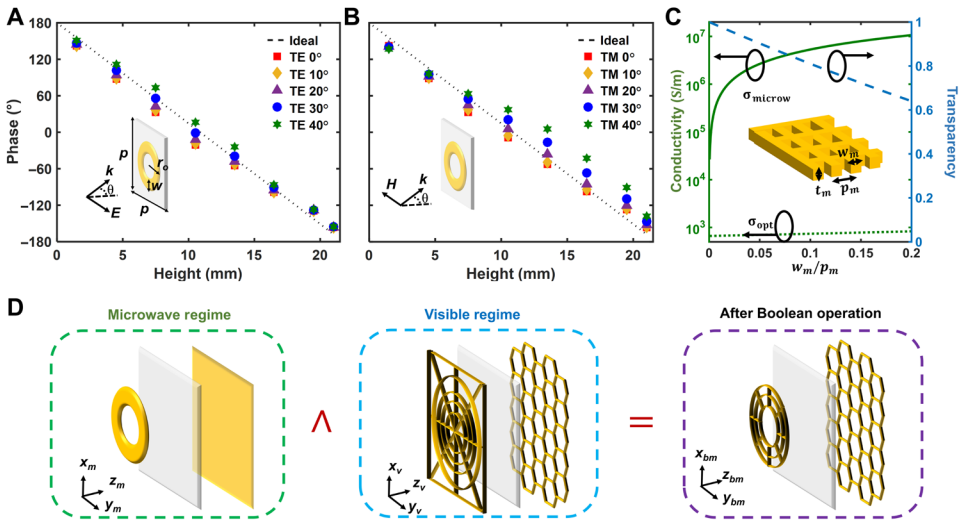

Fig. 2. Boolean metamaterial design procedure for an optically transparent microwave cloak. (**A** and **B**) Schematic of the metasurface unit cell for the microwave regime and the phase shifts under different incident angles: (A) for TE-polarized incidence and (B) for TM-polarized incidence. The dotted line indicates the theoretically ideal phase compensation value at α=10°. (**C**) Cross-scale dispersion engineering with silver nanostructures. The silver ($\omega_p = 1.39 \times 10^{16}$ s^{-1} and $\omega_c = 3.22 \times 10^{13}$ s^{-1}) structure has a geometry of $t_m = 8$ μm and $p_m = 200$ μm, and w_m/p_m varies from 0.001 to 0.2. σ_{microw} and σ_{opt} represent the conductivities at 7 GHz and 580 nm, respectively. The underlying substrate is not considered here. (**D**) Boolean multiplication (denoted by ∧) performed to merge the structures with single-band engineered dispersion into an integrated metastructure with cross-scale engineered dispersion. $M(x_m, y_m, z_m)$, $V(x_v, y_v, z_v)$, and $BM(x_{bm}, y_{bm}, z_{bm})$ are the coordinates for the microwave regime, the visible regime, and the final structure, respectively.

of light, we suppose that all the light that illuminates the silver cannot penetrate the metallic mesh. With this assumption, the light transparency can be estimated by $T = \frac{S_{metal}}{S_{lattice}}$ under normal incidence, and the effective optical conductivity is estimated by $\sigma_{opt} = \sigma_0 \frac{R_{s,mesh}\left(\frac{1}{\sqrt{T}} - 1\right)}{188.5}$ (*33*). Then, an acceptable balance between the contradictory requirements of ultrahigh electrical conductivity at microwave frequencies and ultralow optical conductivity at visible frequencies could be found with a proper w_m/p_m ratio. For instance, $\sigma_{microw} = 2.65 \times 10^6$ S/m and $\sigma_{opt} = 6.98 \times 10^2$ S/m (equivalent to $R_{s,\,mesh} = 0.1$ ohms/□ and $T = 0.95$; see also section S3) can be proposed when $w_m/p_m = 0.025$.

Then, we adopt a Boolean metamaterial design procedure to merge these metastructures for single-band functional realization into an integrated one. For example, to achieve cross-wavelength invisibility with optical transparency and microwave-bypassing ability, we can integrate the metastructures for the microwave regime $M(x_m, y_m, z_m)$ and visible regime $V(x_v, y_v, z_v)$ by adopting a Boolean logical multiplication (denoted by ∧ or AND), i.e., $BM(x_{bm}, y_{bm}, z_{bm}) = M(x_m, y_m, z_m) \wedge V(x_v, y_v, z_v)$, as shown in Fig. 2D. Here, the metastructures in each frequency regime are treated as the inputs of the Boolean AND gate in an integrated circuit. Through this procedure, the integrated metastructures are equal to the macroscopic metallic network formed by mapped microscopic metal wires, which exhibit an extremely high local electrical conductivity while preserving an extremely low global optical conductivity.

The amplitude response of the unit cells is calculated to quantitatively study the potential reflection attenuation with different sheet resistances. From the results in Fig. 3A, one can see that the suitable sheet resistances that match the requirements of the cloak are very limited. When the sheet resistance of the material is outside of this suitable region, the ohmic loss in the unit cells will attenuate the amplitude of the reflected electromagnetic waves and unfavorably deteriorate the cloaking effect (*7*, *34*). Achieving the material parameters that work for our design is very challenging in practice. For example, transparent conducting materials, e.g., indium tin oxides, graphene, and carbon nanowires, usually have good optical transparency only with a higher than 1 ohm/□ sheet resistance (*35*, *36*). However, from the results in Fig. 3A, we find that this kind of metasurface cannot achieve amplitude preservation when the sheet resistance is higher than 1 ohm/□. In other words, such transparent conducting materials may not meet the critical requirements for our cross-wavelength invisibility tactic, although they have been widely used in the demonstration of microwave absorbers (*37*–*40*) and other microwave devices (see section S8). To avoid unnecessary ohmic loss, the width-period ratio w_m/p_m cannot be less than 0.025 locally for the outer-layer metasurface. In addition, considering the vision resolution of the naked eye, we set the width of the metal wires w_m to not exceed 6 μm for the Boolean procedure. The amplitude and phase response of the unit cells after the Boolean procedure are investigated as well. As shown in the inset of Fig. 3A, all the reflection coefficients $|R|$ are close to unity, with the lowest amplitude of the reflection coefficient of 0.89 for ring 5 at 7 GHz. Figure 3 (B and C) presents the phase response of the unit cells at 7 GHz under the illumination of TE waves and TM waves, respectively. The phase responses of all the unit cells are very consistent with the ideal (theoretical) case. Furthermore, the phase response of each unit cell after the Boolean procedure is almost identical to that before the Boolean procedure (Fig. 2, A and B).

Because both a large-area metasurface for concealing macroscopic objects at the microwave scale and high-precision fabrication of microscopic metal wires at the micrometer scale should be guaranteed, an advanced nanoimprinting technique (*28*) is chosen to realize the optically transparent microwave cloak. The optical characterization of the outer-layer and quasi-PEC metasurfaces on PET substrates

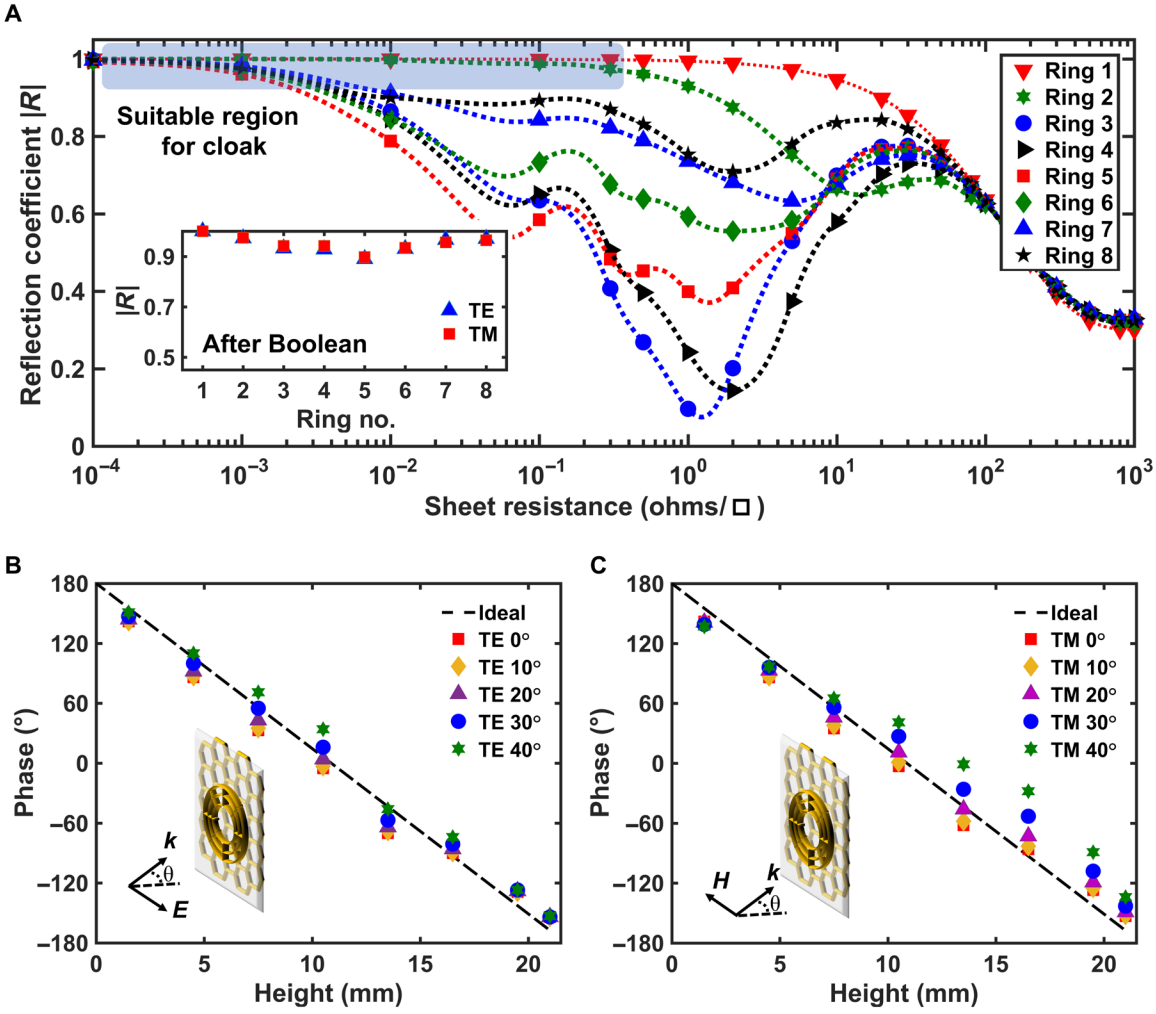

Fig. 3. Phase and amplitude response of ring resonators after the Boolean procedure. (**A**) Amplitude attenuation of a reflected wave for various sheet resistances. The amplitude is averaged under TE polarization incidence (θ = 20 ° and 40°), and the dotted curves are fits from simulations. The inset shows the average magnitude of ring resonators for the practical structure after the Boolean procedure with θ = 0°, 10°, 20°, 30°, and 40° for TE and TM illumination at 7 GHz. (**B** and **C**) Phase responses for TE and TM polarization. The models of the rings after the Boolean procedure are included in fig. S1.

by scanning electron microscopy (SEM) is provided in Fig. 4 (A and B, respectively). The outline of the macroscopic ring resonator is formed by metallic circular wires, and several straight shorting wires oriented along the radial direction are used to connect the circular metal wires. For a ring resonator with a larger width, more concentric circular metal wires could be adopted to preserve the width-period ratio w_m/p_m. In contrast to the ring resonators, hexagonal metal-wire networks are used as the quasi-PEC layer. The microscopic profiles of the interline junctions provided in the insets of Fig. 4 (A and B) present good electrical connections, indicating that the metal wires effectively form macroscopic effective circuits. Because of the metallic networks and good electrical connection, a local high electrical conductivity is achieved over the patterned areas at the microwave scale. The optical transparency is characterized in Fig. 4C. For the case of the outer-layer metasurface, the transmitted light intensity can be higher than 85% over the whole visible wavelength spectrum from 400 to 760 nm, and the highest transmittivity can reach 90% at approximately 660 nm. For the quasi-PEC layer, the average transmitted light intensity is higher than 82% over the full visible range. After stacking up the bilayer metasurface structure, the average transparency could be 72% over the wavelength range from 400 to 760 nm. The optical see-through ability of the optically transparent microwave cloak is experimentally proven in a field test, as shown in Fig. 4D. Compared to the case of direct observation without the cloak (e.g., Fig. 4E), the internal observer can see through the cloak and observe the environment freely with little visual distortion (see movie S1 that mimics the vision of a driver who drives a transparent invisible vehicle).

The microwave cloaking performance is demonstrated experimentally under both TE-polarized and TM-polarized incidence. As shown in Fig. 5A, the reflected beam distributions for the cloak case are identical to those for the ground case shown in Fig. 5B, which indicates that the reflected beam can be recovered when the cloak covers a bump. For comparison to the cloak and ground cases, Fig. 5 (C and D) shows the reflected beam distributions for the case of bumps made from transparent quasi-PEC film and aluminum film, respectively. In both cases, the reflected beams separate into several parts, the patterns of which are completely different from those in the ground

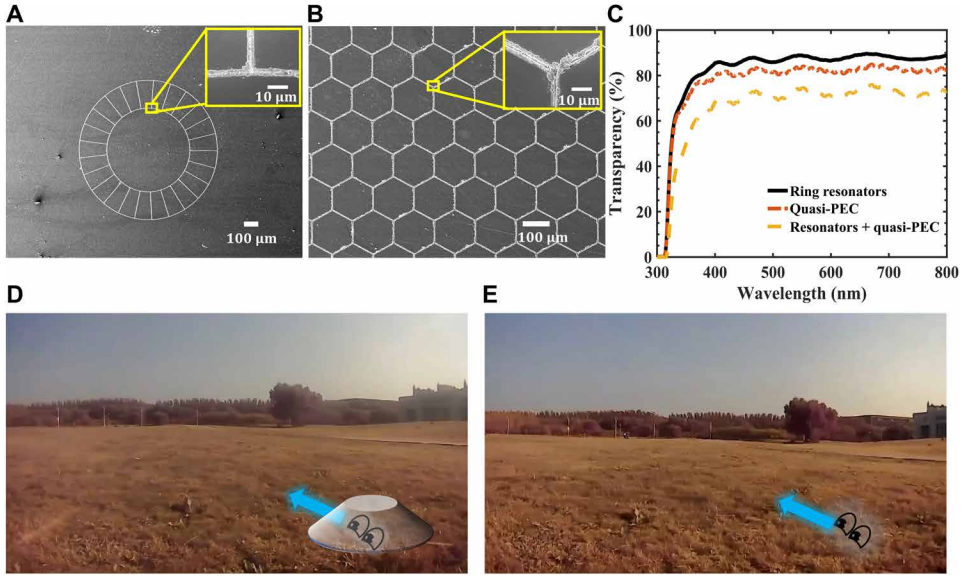

Fig. 4. Optical characterization of the cloak. (**A**) SEM photo of ring 1 with the smallest radius (0.5 mm); scale bar, 100 μm. (**B**) SEM photo of the quasi-PEC layer; scale bar, 100 μm. The insets show a close-up view of the metal wires and their reliable electrical connections; scale bar, 10 μm. (**C**) Optical transparency of the outer-layer metasurface (black solid line), quasi-PEC film (orange dashed-dotted line), and bilayer structure (yellow dashed line). The bilayer transparency equals that of the ring resonators multiplied by that of the quasi-PEC film. (**D**) Experimental proof of how an internal observer sees through the cloak compared to (**E**) the case of direct observation without the cloak. Photo credit: Fu-Yan Dong and Dong-Dong Han, Jilin University.

case. One can see that the reflected beam distribution for the case of the transparent PEC is almost identical to that for the case of the aluminum bump, which provides unambiguous evidence that the metallic networks have extremely high conductivity and can act as quasi-PECs at microwave frequencies. The experimental results of the reflected beam distributions under TM-polarized incidence at 7 GHz are plotted in Fig. 5 (F to I). Similar to the TE cases, the reflected magnetic field distributions for the cloak case are in good agreement with those for the flat ground case.

Furthermore, the total scattering reduction for our sample over different frequencies is studied experimentally. The total scattering reductions are calculated through $\sigma_{\text{reduction,TE}} = \frac{\sigma_{\text{cloaked,TE}}}{\sigma_{\text{bare,TE}}} = \frac{\int(E_{z,\text{cloaked}} - E_{z,\text{ground}})\,d\varnothing}{\int(E_{z,\text{bare}} - E_{z,\text{ground}})\,d\varnothing}$ for the TE case, shown in Fig. 5E, and $\sigma_{\text{reduction,TM}} = \frac{\sigma_{\text{cloaked,TM}}}{\sigma_{\text{bare,TM}}} = \frac{\int(H_{z,\text{cloaked}} - H_{z,\text{ground}})\,d\varnothing}{\int(H_{z,\text{bare}} - H_{z,\text{ground}})\,d\varnothing}$ for the TM case, shown in Fig. 5J. Here, ∅ represents the azimuthal angle from −90° to 90°. Both the electric field and magnetic field are in complex form, i.e., $E_z = E_{Rz} + iE_{Iz}$ and $H_z = H_{Rz} + iH_{Iz}$, where subscripts *R* and *I* represent the real part and imaginary parts, respectively, of the electric field and magnetic field. The substantial reduction of the total scattering also indicates that the phase and amplitude of the wave reflected from the cloak is the same as those of the wave reflected from the ground plane (*12*, *19*). For the TE case, the cloak can decrease the total scattering of the object over the frequency range from 6 to 10 GHz, where the best 3-dB bandwidth is approximately 27.9% (from 6.65 to 8.81 GHz, α = 6°). Furthermore, the total scattering can be decreased to 14.5% at 7.57 GHz when α = 6°, which is shifted slightly compared to the designed frequency (i.e., 7 GHz) and designed incident angle (α = 10°). For the TM case, the total scattering can be decreased to 25.0% at 7.16 GHz and α = 16°, which is slightly higher than that in the TE case. The best 3-dB bandwidth in the TM case is approximately 18.9% (from 6.46 to 7.81 GHz, α = 16°). In addition, the numerical electromagnetic field distribution away from the cloak and the experimental differential scattering of the cloak (*19*) are provided in figs. S2 and S8, respectively.

DISCUSSION

The above results indicate achievement of cross-wavelength invisibility with preserved amplitude and undistorted phase at microwave frequencies, as well as omnidirectional transparency over the visible spectrum. Compared to previous carpet cloaks (*14*–*27*), our work presents an experimental demonstration of achieving invisibility over cross-wavelength wide regimes by integrating various invisibility tactics. Our work not only exhibits the advantages of polarization independence (*15*, *19*–*21*, *24*), wide incident angle allowance (*21*, *24*, *26*, *27*), and remarkable bandwidth (*14*, *15*, *17*–*22*, *24*–*26*) in the cloaking/longwave region but also features body transparency in the shortwave region. Such cross-wavelength invisibility integration is in line with the technical trend of stealth technology and can be practically more available with advanced nanofabrication technologies. Longwave detection is the technical trend of advanced long-distance detection technologies, because electromagnetic waves with longer wavelengths can propagate over a larger distance even in severe weather. In contrast to long waves, short waves cannot propagate over these long distances but are very helpful for people seeking a high resolution. The combination of longwave cloaking and shortwave transparency allows the eyes of a stealth system to clearly observe the external world while the system remains undetectable. Furthermore, it is possible to integrate transparent components underneath our cloak to enable a comprehensive system (see section S8).

On the basis of previous methods for controlling electromagnetic waves (*1*, *3*–*11*), our Boolean metamaterial design procedure provides the possibility to combine various invisibility tactics, which is

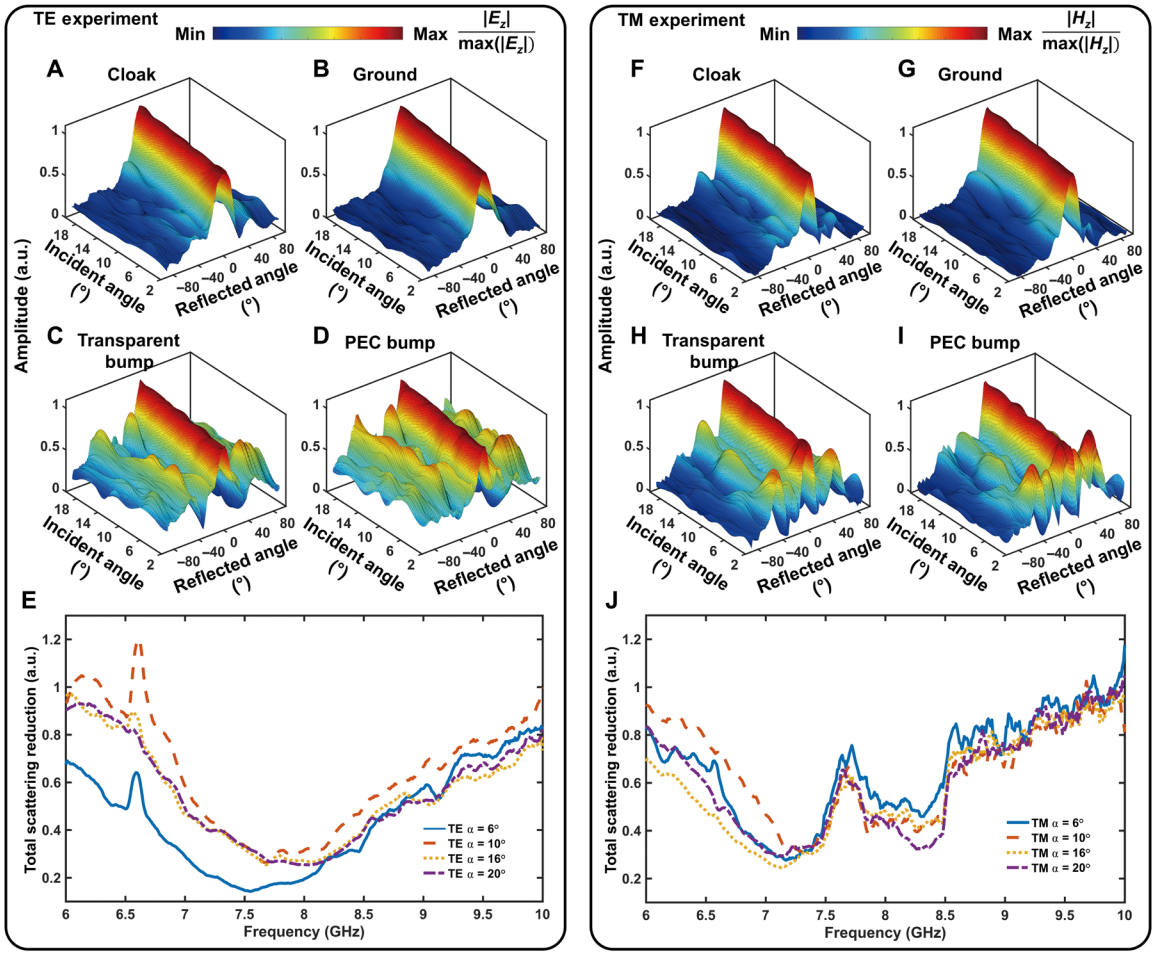

Fig. 5. Experimental results in the microwave regime for the TE case (left column) and TM case (right column). Amplitude distribution of the reflected waves: (**A** and **F**) cloak, (**B** and **G**) ground, (**C** and **H**) transparent bump made from a transparent quasi-PEC layer, and (**D** and **I**) PEC bump made from aluminum. (**E** and **J**) Total scattering reduction with $\alpha = 6°$ (solid line), 10° (dashed line), 16° (dotted line), and 20° (dash-dotted line). The distributions are plotted for the incident angle α from 2° to 20° and reflected angle ϕ from −90° to 90° at 7 GHz. a.u., arbitrary units.

a general-purpose methodology for cross-wavelength invisibility integration. Moreover, triggered by the concept of integrated logic circuits, our work may eliminate concerns regarding compact designs with divergent functional requirements and thereby pave the way toward the integrated realization of multifunctional or even multiphysics devices with compact dimensions.

MATERIALS AND METHODS

Boolean metamaterial design procedure

Here, we experimentally demonstrate the cross-wavelength invisibility device as only one example of the Boolean metamaterial design procedure. More generally, this procedure can be expressed as

$$R_t(x,y,z) = BF(R_1(x,y,z), R_2(x,y,z),\ldots,R_N(x,y,z)) \quad (1)$$

where R_t is the target metastructure, R_i ($N = 1,2, \ldots, N$) is the metastructure of the Nth function/frequency regime, and "BF" represents the Boolean functions (e.g., AND, OR, and NOR) or their logical combinations adopted for the corresponding metastructures. In the first step of the procedure, metastructures with divergent spectral responses are achieved individually in their corresponding frequency regime. In this step, the metastructures in each frequency regime are treated as the inputs of relevant Boolean gates in an integrated circuit. As long as the functionality of the metastructures is dispersion independent, we can merge the geometries of the metastructures with single-band engineered dispersion into an integrated structure with multiband engineered dispersive properties following suitable Boolean operations or their combinations. Last, practical multifunctional or multifrequency devices based on Boolean metamaterials can be realized with the use of proper advanced nanofabrication technologies to support the multilevel geometrical degree of freedom in Boolean metamaterials. More details of this procedure are discussed in section S4.

Fabrication

The transparent metasurfaces are fabricated through an advanced nanoimprinting technique, the procedure of which is illustrated in fig. S6. First, photolithography is used to produce a Ni master plate with convex patterns as the imprinting template. Second, a layer of

ultraviolet (UV) glue is used to cover a PET substrate, and then, the Ni master plate is imprinted into the UV glue layer (fig. S6A). This step is carried out to form grooves with high aspect ratios, as shown in fig. S6B. Third, nano-Ag ink is poured into the grooves as the electroplating seed layer shown in fig. S6C. Last, metallic Ni is electroplated on top of the microscopic Ag wires inside the grooves (fig. S6D). The proposed electroplating step is performed to further increase the height of the microscopic metal wires, which could decrease the sheet resistance. The purpose of using Ag is to realize extremely low sheet resistance with relatively low loss in visible transmittance, while electroplating of Ni is carried out to prevent the Ag-based metasurface from being oxidized, expecting to obtain a long service life in practical application scenarios. The width, period, and arrangement of the metal wires are optimized slightly in the fabrication.

Microwave experiment

All the microwave measurements are carried out in a microwave absorber chamber, and a schematic view of the microwave experimental setup is illustrated in fig. S7. All the original experimental data are obtained automatically with the use of a Linbou three-dimensional near-field scanning system. A laptop with the measurement operation system and postprocessing software is connected simultaneously to a Keysight E5071C vector network analyzer (VNA) and an electrical control box by cables. Two ports of the VNA are connected to a horn antenna as the transceiver and a probe as the receiver. The transmitting antenna used in the experiment is an HD-100LHA250SZJ high-gain directive horn antenna from Xi'an Hengda Microwave Technology Development Co. Ltd. A monopole probe is used to detect the electric field for TE-polarized incidence, while a commercial 100A Beehive EMC (electromagnetic compatibility) probe is used to detect the magnetic field for TM-polarized incidence. During the measurement, a half-circular path of $\varnothing \in (-90°, 90°)$ with a radius of 250 mm is used to obtain the reflected fields. The azimuthal resolution is 1° in the experiment.

Optical characterization

Both the outer-layer and inner-layer metasurfaces are cut into small pieces for optical characterization. A UV-visible spectrophotometer (UV-2550) is adopted to determine the transmitted light intensities, and a JSM-7500F SEM is used to observe the microscopic geometries of metal wires. The sheet resistance of the quasi-PEC layer is determined with the use of a four-probe detector (ST-21H, 4 Probes Tech). A micro wireless surveillance camera (JOOAN JA-A4) is used in the field test to mimic the vision of a driver inside an optically transparent microwave invisibility cloak (car).

SUPPLEMENTARY MATERIALS

Supplementary material for this article is available at http://advances.sciencemag.org/cgi/content/full/6/39/eabb3755/DC1

REFERENCES AND NOTES

1. T. W. Cronin, Camouflage: Being invisible in the open ocean. *Curr. Biol.* **26**, R1177–R1196 (2016).
2. P. Barbosa, I. Castellanos, *Ecology of Predator-Prey Interactions* (Oxford Univ. Press, 2005).
3. M. Vatankhah-Varnosfaderani, A. N. Keith, Y. Cong, H. Liang, M. Rosenthal, M. Sztucki, C. Clair, S. Magonov, D. A. Ivanov, A. V. Dobrynin, S. S. Sheiko, Chameleon-like elastomers with molecularly encoded strain-adaptive stiffening and coloration. *Science* **359**, 1509–1513 (2018).
4. J. Teyssier, S. V. Saenko, D. van der Marel, M. C. Milinkovitch, Photonic crystals cause active colour change in chameleons. *Nat. Commun.* **6**, 6368 (2015).
5. C. Xu, G. T. Stiubianu, A. A. Gorodetsky, Adaptive infrared-reflecting systems inspired by cephalopods. *Science* **359**, 1495–1500 (2018).
6. C. Yu, Y. Li, X. Zhang, X. Huang, V. Malyarchuk, S. Wang, Y. Shi, L. Gao, Y. Su, Y. Zhang, H. Xu, R. T. Hanlon, Y. Huang, J. A. Rogers, Adaptive optoelectronic camouflage systems with designs inspired by cephalopod skins. *Proc. Natl. Acad. Sci. U.S.A.* **111**, 12998–13003 (2014).
7. J. B. Pendry, D. Schurig, D. R. Smith, Controlling electromagnetic fields. *Science* **312**, 1780–1782 (2006).
8. U. Leonhardt, Optical conformal mapping. *Science* **312**, 1777–1780 (2006).
9. J. Li, J. B. Pendry, Hiding under the carpet: A new strategy for cloaking. *Phys. Rev. Lett.* **101**, 203901 (2008).
10. N. Yu, P. Genevet, M. A. Kats, F. Aieta, J.-P. Tetienne, F. Capasso, Z. Gaburro, Light propagation with phase discontinuities: Generalized laws of reflection and refraction. *Science* **334**, 333–337 (2011).
11. A. Alù, N. Engheta, Achieving transparency with plasmonic and metamaterial coating. *Phys. Rev. E* **72**, 016623 (2005).
12. B. Edward, A. Alù, M. G. Silveirinha, N. Engheta, Experimental verification of plasmonic cloaking at microwave frequencies with metamaterials. *Phys. Rev. Lett.* **103**, 153901 (2009).
13. D. Schurig, J. J. Mock, B. J. Justice, S. A. Cummer, J. B. Pendry, A. F. Starr, D. R. Smith, Metamaterial electromagnetic cloak at microwave frequencies. *Science* **314**, 977–980 (2006).
14. R. Liu, C. Ji, J. J. Mock, J. Y. Chin, T. J. Cui, D. R. Smith, Broadband ground-plane cloak. *Science* **323**, 366–369 (2009).
15. H. F. Ma, T. J. Cui, Three-dimensional broadband ground-plane cloak made of metamaterials. *Nat. Commun.* **1**, 21 (2010).
16. N. Landy, D. R. Smith, A full-parameter unidirectional metamaterial cloak for microwaves. *Nat. Mater.* **12**, 25–28 (2013).
17. D. Shin, Y. Urzhumov, Y. Jung, G. Kang, S. Baek, M. Choi, H. Park, K. Kim, D. R. Smith, Broadband electromagnetic cloaking with smart metamaterials. *Nat. Commun.* **3**, 1213 (2012).
18. B. Orazbayev, N. Mohammadi Estakhri, M. Beruete, A. Alù, Terahertz carpet cloak based on a ring resonator metasurface. *Phys. Rev. B* **91**, 195444 (2015).
19. Y. Yang, L. Jing, B. Zheng, R. Hao, W. Yin, E. Li, C. M. Soukoulis, H. Chen, Full-polarization 3D metasurface Cloak with preserved amplitude and phase. *Adv. Mater.* **28**, 6866–6871 (2016).
20. J. Yang, C. Huang, X. Wu, B. Sun, X. Luo, Dual-wavelength carpet cloak using ultrathin metasurface. *Adv. Opt. Mater.* **6**, 1800073 (2018).
21. B. Orazbayev, N. Mohammadi Estakhri, A. Alù, M. Beruete, Experimental demonstration of metasurface-based ultrathin carpet cloaks for millimeter waves. *Adv. Opt. Mater.* **5**, 1600606 (2017).
22. J. Valentine, J. Li, T. Zentgraf, G. Bartal, X. Zhang, An optical cloak made of dielectrics. *Nat. Mater.* **8**, 568–571 (2009).
23. L. H. Gabrielli, J. Cardenas, C. B. Poitras, M. Lipson, Silicon nanostructure cloak operating at optical frequencies. *Nat. Photon.* **3**, 461–463 (2009).
24. T. Ergin, N. Stenger, P. Brenner, J. B. Pendry, M. Wegener, Three-dimensional invisibility cloak at optical wavelengths. *Science* **328**, 337–339 (2010).
25. B. Zhang, Y. Luo, X. Liu, G. Barbastathis, Macroscopic invisibility cloak for visible light. *Phys. Rev. Lett.* **106**, 033901 (2011).
26. X. Chen, Y. Luo, J. Zhang, K. Jiang, J. B. Pendry, S. Zhuang, Macroscopic invisibility cloaking of visible light. *Nat. Commun.* **2**, 176 (2011).
27. X. Ni, Z. J. Wong, M. Mrejen, Y. Wang, X. Zhang, An ultrathin invisibility skin cloak for visible light. *Science* **349**, 1310–1314 (2015).
28. X. Chen, S. Nie, W. Guo, F. Fei, W. Su, W. Gu, Z. Cui, Printable high-aspect ratio and high-resolution Cu grid flexible transparent conductive film with figure of merit over 80000. *Adv. Electron. Mater.* **5**, 1800991 (2019).
29. A. J. Peacock, *Handbook of Polyethylene: Structure, Properties, and Applications* (Marcel Dekker Inc., 2000).
30. B. Zhang, T. Chan, B.-I. Wu, Lateral shift makes a ground-plane cloak detectable. *Phys. Rev. Lett.* **104**, 233903 (2010).
31. P. B. Johnsom, R. W. Christy, Optical constants of the noble metals. *Phys. Rev. B* **6**, 4370–4379 (1972).
32. P. B. Catrysse, S. Fan, Nanopatterned metallic films for use as transparent conductive electrodes in optoelectronic devices. *Nano Lett.* **10**, 2944–2949 (2010).
33. M. Dressel, G. Grüner, *Electrodynamics of Solids: Optical Properties of Electrons in Matter* (Cambridge Univ. Press, 2002).
34. H. Hashemi, B. Zhang, J. D. Joannopoulos, S. G. Johnson, Delay-bandwidth and delay-loss limitations for cloaking of large objects. *Phys. Rev. Lett.* **104**, 243903 (2010).
35. Y. Zhang, S.-W. Ng, X. Lu, Z. Zheng, Solution-processed transparent electrodes for emerging thin-film solar cells. *Chem. Rev.* **120**, 2049–2122 (2020).
36. D. Zhang, T. Huang, L. Duan, Emerging self-emissive technologies for flexible displays. *Adv. Mater.* **32**, 1902391 (2020).

37. C. Zhang, J. Yang, W. Cao, W. Yuan, J. Ke, L. Yang, Q. Cheng, T. Cui, Transparently curved metasurface with broadband millimeter wave absorption. *Photonics Res.* **7**, 478–485 (2019).
38. T. Jang, H. Youn, Y. J. Shin, L. J. Guo, Transparent and flexible polarization-independent microwave broadband absorber. *ACS Photonics* **1**, 279–284 (2014).
39. K. Chen, L. Cui, Y. Feng, J. Zhao, T. Jiang, B. Zhu, Coding metasurface for broadband microwave scattering reduction with optical transparency. *Opt. Express* **25**, 5571–5579 (2017).
40. G. Song, C. Zhang, Q. Cheng, Y. Jing, C. Qiu, T. Cui, Transparent coupled membrane metamaterials with simultaneous microwave absorption and sound reduction. *Opt. Express* **26**, 22916–22925 (2018).
41. Y. Liu, J. Tan, Experimental study on a resonance mesh coating fabricated using a UV-lithography technique. *Opt. Express* **21**, 4228–4234 (2013).
42. C. Tsakonas, S. C. Liew, C. Mias, D. C. Koutsogeorgis, R. M. Ranson, W. M. Cranton, M. Dudhia, Optically transparent frequency selective window for microwave applications. *Electron. Lett.* **37**, 1464–1466 (2001).
43. A. Katsounaros, Y. Hao, N. Collings, W. A. Crossland, Optically transparent ultra-wideband antenna. *Electron. Lett.* **45**, 722–723 (2009).
44. T. Peter, T. A. Rahman, S. W. Cheung, R. Nilavalan, H. F. Abutarboush, A. Vilches, A novel transparent UWB antenna for photovoltaic solar panel integration and RF energy harvesting. *IEEE Trans. Antennas Propag.* **62**, 1844–1853 (2014).
45. J. van de Groep, P. Splinelli, A. Polman, Transparent conducting silver nanowire networks. *Nano Lett.* **12**, 3138–3144 (2012).
46. Y. Yang, S. Jeong, L. Hu, H. Wu, S. W. Lee, Y. Cui, Transparent lithium-ion batteries. *Proc. Natl. Acad. Sci. U.S.A.* **108**, 13013–13018 (2011).
47. S. Chun, W. Son, G. Lee, S. H. Kim, J. W. Park, S. J. Kim, C. Pang, C. Choi, Single-layer graphene-based transparent and flexible multifunctional electronics for self-charging power and touch-sensing systems. *ACS Appl. Mater. Interfaces* **11**, 9301–9308 (2019).
48. J. Yao, J. Lin, Y. Dai, G. Ruan, Z. Yan, L. Li, L. Zhong, D. Natelson, J. M. Tour, Highly transparent nonvolatile resistive memory devices from silicon oxide and graphene. *Nat. Commun.* **3**, 1101 (2012).
49. P. K. Nayak, Z. Wang, H. N. Alshareef, Indium-free fully transparent electronics deposited entirely by atomic layer deposition. *Adv. Mater.* **28**, 7736–7744 (2016).
50. P. Li, Y. Wang, U. Gupta, J. Liu, L. Zhang, D. Du, C. C. Foo, J. Ouyang, J. Zhu, Transparent soft robots for effective camouflage. *Adv. Funct. Mater.* **29**, 1901908 (2019).

Acknowledgments: We thank Q.-D. Chen, X.-L. Zhang, Z.-J. Wang, and Z.-J. Yang for helpful discussion. **Funding:** This work was sponsored by the National Natural Science Foundation of China (NSFC) grant nos. 61805097, 61935015, 61590930, 61825502, and 61801426; the National Key R&D Program of China grant 2017YFB1104300; and ZJNSF grant LZ20F010007. C.Q. and H.C. acknowledge the support from the NSFC under grant nos. 61625502, 11961141010, and 61975176. **Author contributions:** S.X. and H.C. conceived the original idea. S.X. designed the device and performed the analytical calculation and numerical simulations. F.-Y.D. and D.-D.H. conducted the experiment. W.-R.G. and W.-M.S. fabricated the sample. C.Q. provided technical support for the experiment and revised the manuscript. S.X., F.G., H.C., and H.-B.S. analyzed the data, interpreted the results, and wrote the manuscript. All the authors reviewed and discussed the manuscript. **Competing interests:** The authors declare that they have no competing interests. **Data and materials availability:** All data needed to evaluate the conclusions in the paper are present in the paper and/or the Supplementary Materials. Additional data related to this paper may be requested from S.X., H.C., and H.-B.S.

Submitted 19 February 2020
Accepted 4 August 2020
Published 23 September 2020
10.1126/sciadv.abb3755

Citation: S. Xu, F.-Y. Dong, W.-R. Guo, D.-D. Han, C. Qian, F. Gao, W.-M. Su, H. Chen, H.-B. Sun, Cross-wavelength invisibility integrated with various invisibility tactics. *Sci. Adv.* **6**, eabb3755 (2020).